Journal of Alloys and Compounds 503 (2010) 25–30

Contents lists available at ScienceDirect

Journal of Alloys and Compounds

journal homepage: www.elsevier.com/locate/jallcom

Interfacial reactions on Pb-free solders with Au/Pd/Ni/Cu multilayer substrates

Yee-wen Yen[a,b,*], Po-hao Tsai[c], Yang-kai Fang[c], Shao-cheng Lo[a], Yu-Ping Hsieh[a], Chiapyng Lee[c]

[a] Graduate Institute of Engineering, National Taiwan University of Science and Technology, Taipei 106, Taiwan
[b] Department of Polymer Engineering, National Taiwan University of Science and Technology, Taipei 106, Taiwan
[c] Department of Chemical Engineering, National Taiwan University of Science and Technology, Taipei 10672, Taiwan

ARTICLE INFO

Article history:
Received 18 March 2010
Received in revised form 7 April 2010
Accepted 7 April 2010
Available online 6 May 2010

Keywords:
Interfacial reaction
Lead-free solder
Au/Pd/Ni/Cu multilayer substrate
Diffusion-controlled
Activation energy

ABSTRACT

In this study, the interfacial reactions on Sn, Sn–3.0Ag–0.5Cu, Sn–0.7Cu, Sn–58Bi and Sn–9Zn lead-free solders with the Au/Pd/Ni/Cu multilayer substrate at 240–270 °C for 20 min to 20 h were investigated. The experimental results showed that the $(Ni, Cu)_3Sn_4$ phase is converted to the $(Cu, Ni)_6Sn_5$ and Cu_3Sn phases in the Sn/Au/Pd/Ni/Cu system when the reaction time is longer than 4 h. In Sn–3.0Ag–0.5Cu/Au/Pd/Ni/Cu and Sn–0.7Cu/Au/Pd/Ni/Cu systems, the $(Cu, Ni)_6Sn_5$ and Cu_3Sn phase were observed, and only the Ni_3Sn_4 phase was formed at the Sn–58Bi/Au/Pd/Ni/Cu interface. Furthermore, the Pd_2Zn_9 and NiZn phases were formed in the Sn–9Zn/Au/Pd/Ni/Cu system. When the reaction time was longer than 4 h, the Pd_2Zn_9, NiZn, and Ni_5Zn_{21} phases were formed at the interface. The reaction mechanism for all the reaction systems was diffusion-controlled. The Sn–58Bi/Au/Pd/Ni/Cu system was found to have the lowest activation energy when compared with other systems, and its value was 17.43 kJ/mol.

© 2010 Elsevier B.V. All rights reserved.

1. Introduction

With the electronic products becoming lighter and smaller with higher performance and high I/O (In/Out) density, the micro-interconnection technology adopted between the electronic devices and substrates has become increasingly more important. As the conventional Sn–Pb solders have excellent soldering characteristics and reliability [1,2], Sn–Pb solders have been widely used in the soldering processes for several decades. However, Pb is a toxic metal, and its compounds are harmful to human health [3]. In recent years, owing to the increase in the global environmental consciousness and aggressive passing of related Pb-banning laws by the European Union, such as WEEE and RoHS, conventional Sn–Pb solders have been replaced by Pb-free solders since July 1, 2006 [4]. Many Pb-free solders have been developed, such as pure Sn, Sn–3.0 wt% Ag–0.5 wt% Cu (SAC), Sn–0.7 wt% Cu (SC), Sn–58.0 wt% Bi (SB) and Sn–9.0 wt% Zn (SZ), which are the most promising Pb-free solders [5–10].

SAC solder is suitable for flip-chip (FC) and ball grid array (BGA) reflowing process [7], and SC solder is suitable for wave soldering [6,9]. Both SAC and SC solders provide good mechanical properties and solderability. As the eutectic temperature of SB solder is 139 °C, it is suitable for communication and consumer electronic products, and both the joint reliability and cost of SB solder are close to those of the conventional Sn–Pb solders [10]. The eutectic temperature of SZ solder is 198 °C, which is very close to the melting temperature of the Sn–37Pb solder (183 °C). Furthermore, beside the lower process discrepancy between SZ and Sn–37Pb solder, SZ solder is observed to demonstrate better mechanical properties than the Sn–37Pb solder [8].

Pb-free solders are used for bonding devices onto the substrates as well as in printed circuit boards for surface-finishing treatment [11–13]. To improve the joint reliability and wettability between the solder and the substrate, the used of Au/Ni, Pd/Ni, and Au/Pd/Ni layer structures on copper is the most common approach for surface-finishing treatment [14]. The Au layer provides oxidation resistant and better wettability between the solder and the pad. The Pd layer improves the wettability and acts as a diffusion barrier as well. The Ni layer is widely adopted as a diffusion barrier material to prevent the rapid reaction between the Cu and solder induced by Cu diffusion.

Although numerous efforts have been made to study the interfacial reactions of Pb-free solders with Cu or Ni substrates, research on the interfacial reactions between the solder and Au/Pd/Ni/Cu multilayer substrate systems is still lacking. In this study, the liquid/solder reaction couple technique has been used to investigate the interfacial reactions of the Au/Pd/Ni/Cu multilayer substrate in molten Sn, Sn–3.0 wt% Ag–0.5 wt% Cu, Sn–58.0 wt% Bi and Sn–9.0 wt% Zn Pb-free solders at 240, 255, and 270 °C for various periods of reaction times.

* Corresponding author at: Graduate Institute of Engineering, National Taiwan University of Science and Technology, No. 43, Keelung Section 4, Taipei 106, Taiwan. Tel.: +886 2 27376659; fax: +886 2 27301265.
E-mail address: ywyen@mail.ntust.edu.tw (Y.-w. Yen).

0925-8388/$ – see front matter © 2010 Elsevier B.V. All rights reserved.
doi:10.1016/j.jallcom.2010.04.241

Table 1
Compositions of etching solutions for different solder/substrate systems.

Solders	Sn/SC/SZ	SAC	SB
Etchant	CH_3OH:HCl:HNO_3	CH_3OH:HCl	HNO_3:H_2O
Ratio (vol.%)	93:2:5	9:1	1:1

2. Experimental

Individual Cu multilayer substrates were electroplated with 75 nm-thick Au layer, 210 nm-thick Pd layer, and 1.78 μm-thick Ni layer, respectively. The Au/Pd/Ni/Cu multilayer substrate with 15.0 mm × 5.0 mm × 1.0 mm was ultrasonically cleaned in ethanol and then dipped in diluted HCl solution. The substrate was ultrasonically rinsed in de-ionized water to ensure that there was no contamination on the substrate surface. The Sn, SAC, SC, SB and SZ solders were prepared with Sn, Ag, Cu, Bi and Zn shots of above 99.0 wt% purity. In particular, for this study, the liquid/solid reaction couples were prepared. The cleaned Au//Pd/Ni/Cu multilayer substrate was dipped in a rosin mildly activated (RMA) flux and reacted with solders in an evacuated quartz tube. The couples were placed in a tube furnace at 240, 255 and 270 °C for 20 min to 20 h.

After the completion of the solid/liquid interfacial reactions, all the couples were subsequently quenched in ice water. A metallurgical treatment was first applied to make the cross-sectional interface perpendicular to the exposed substrates. To elucidate the relationship between the surface morphology and intermetallic compound (IMC) microstructure, deep-etching technique was employed to study the microstructures of the interface between the solder and the substrate. The couples were etched with different etching solutions for a few minutes to remove the solder. The detailed etching solution compositions for each solder/substrate couple are listed in Table 1. Thus, the 3-D microstructure of the IMCs formed at the interface can be clearly observed. Optical microscope (OM) and scanning electron microscope (SEM) were used for microstructure examination. SEM with an energy dispersive spectrometer (EDS) and electron probe micro-analyzer (EPMA) were used to determine the IMC composition and the results were compared with the related phase diagrams. The IMCs formed at the solder/substrate interface was identified using both the data.

3. Results and discussion

3.1. Sn/Au/Pd/Ni/Cu reaction couple

Fig. 1(a) shows a backscatter electron image (BEI) of the Sn solder reacting with the Au/Pd/Ni/Cu substrate at 270 °C for 1 h. It can be observed that the Au and Pd layers are completely dissolved into the molten Sn solder, which is owing to their thinness. As shown in Fig. 1(a), a light gray and scallop-shaped layer is formed at the Sn side. The EPMA analysis revealed that its composition is Sn–37.2Cu–16.3Ni (at.%). Based on the Sn-Cu, Ni-Sn binary phase diagram [15,16] and Sn–Cu–Ni ternary phase diagram [17], this is considered to be the (Cu, Ni)$_6$Sn$_5$ phase, which has 16.3 at.% Ni solubility with Cu_6Sn_5 phase. A dark-gray and discontinuous

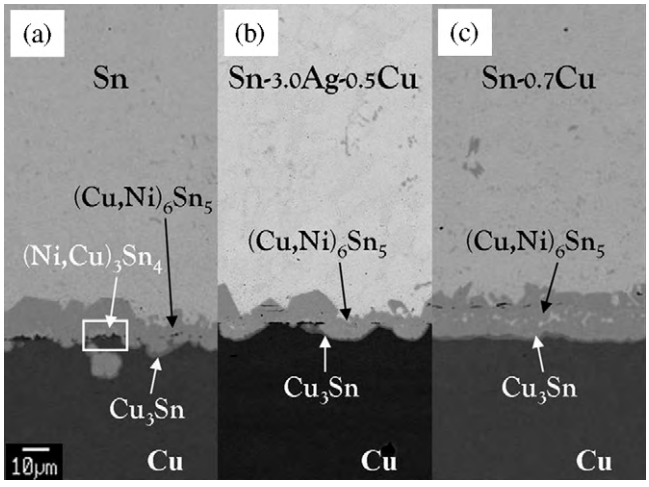

Fig. 1. BEI micrograph of the (a) Sn/Au/Pd/Ni/Cu, (b) SAC/Au/Pd/Ni/Cu and (c) SC/Au/Pd/Ni/Cu reaction couples reacted at 270 °C for 1 h.

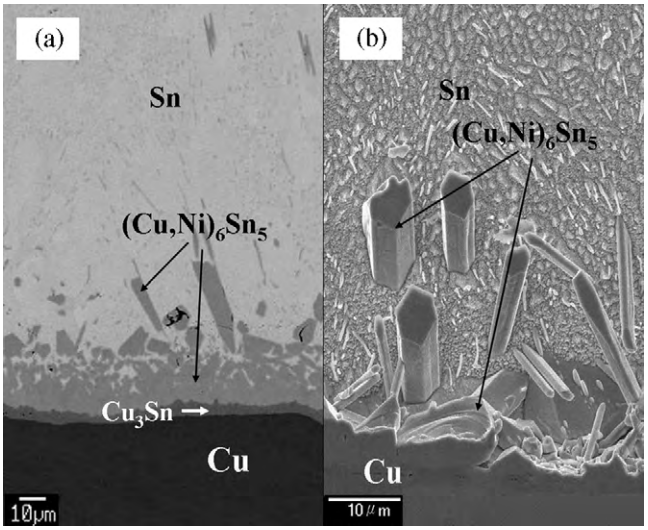

Fig. 2. (a) Un-etched and (b) deep-etched BEI microstructure of the Sn/Au/Pd/Ni/Cu reaction couple reacted at 270 °C for 4 h.

layer closed to the Cu side was found and its composition was Cu–22.4 at.% Sn. This is likely to be the Cu_3Sn phase [15]. A bright-colored thin layer with the composition of Sn–35.6Ni–8.7Cu (at.%) determined from EPMA analysis, was formed between the (Cu, Ni)$_6$Sn$_5$ and Cu_3Sn phases, which is likely to be (Ni, Cu)$_3$Sn$_4$ phase [17]. In this case, a few Ni layer still remained on the Cu surface. Similar results were found when the reaction temperatures were reduced to 255 or 240 °C for various reaction times.

When the reaction time was extended to 4 h, the Ni layer was completely consumed. As shown in Fig. 2(a), only the (Cu, Ni)$_6$Sn$_5$ and Cu_3Sn phases were formed at the interface and no Ni–Sn IMCs were found. The IMC at the Sn side was loose and peeled off the interface. According to the EPMA analysis, this should be the $(Cu_{0.59}Ni_{0.41})_6Sn_5$ phase. Furthermore, the inner IMC near and close to the Cu_3Sn phase was much denser than the spalling IMC, which was the $(Cu_{0.84}Ni_{0.16})_6Sn_5$ phase. When the reaction time was increased, the small grain size of the (Cu, Ni)$_6$Sn$_5$ phases ripened to form a greater one to reduce the free energy. Thus, the larger grain size of the (Cu, Ni)$_6$Sn$_5$ phase exhibited continuous growth. This result was very similar to that obtained in the interfacial reaction between the liquid Sn and solid Cu substrate, which formed the Cu_6Sn_5 and Cu_3Sn phases in this reaction system [18].

For a clear observation of the 3-D IMC morphology, the etching solution was used to remove the solder for each reaction couple. Fig. 2(b) shows a deep-etched SEI micrograph of the Sn/Au/Pd/Ni/Cu couple reacted at 270 °C for 4 h. Furthermore, the grain morphology of the (Cu, Ni)$_6$Sn$_5$ phase in the solder showed a hexagonal polyhedron-type shape, which is different from the other Cu_6Sn_5 phase that was close to the Cu_3Sn phase and exhibited a cobble shape. Similar results were found when the reaction temperatures were decreased to 240 and 255 °C. This indicates that that the temperature change does not significantly influence IMC formation.

The reaction mechanism for the Sn/Au/Pd/Ni/Cu system is that Au and Pd atoms rapidly dissolved into the molten Sn. However, the concentrations of Au and Pd are too limited to be detected. The Sn atoms were found to diffuse into the substrate side and react with the Ni and Cu sides to form the Ni_3Sn_4 and Cu_6Sn_5 phases, respectively. The high Cu-concentration IMC, the Cu_3Sn phase, was formed at the Cu side. However, the Ni supply was not limitless. When the Ni layer was consumed completely, more Cu atoms diffused toward the solder side and were incorporated into the sublattice of the Ni_3Sn_4 phase. Meanwhile, the Cu diffusion rate in Sn was faster than the Ni diffusion rate in the Sn [19]. Thus, it can

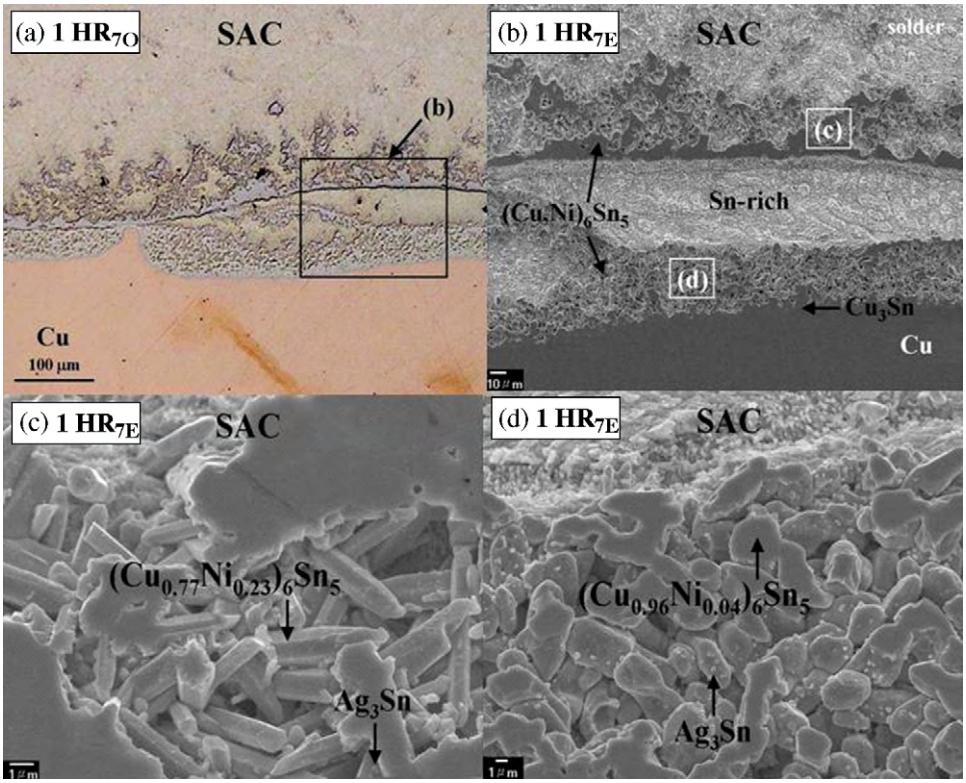

Fig. 3. (a) Un-etched optical micrograph and (b) deep-etched BEI micrograph of the SAC/Au/Pd/Ni/Cu reaction couple reacted at 270 °C for 1 h; (c), (d) is magnified locally from (b).

be concluded that the Ni_3Sn_4 phase was converted to the Cu_6Sn_5 phase, which explains why about 22.6 at.% Ni had solid solubility in the (Cu, Ni)$_6Sn_5$ phase, which is close to the solder side. However, only about 8.8 at.% Ni in the (Cu, Ni)$_6Sn_5$ phase was near the substrate side.

3.2. Sn–3.0Ag–0.5Cu/Au/Pd/Ni/Cu reaction couple

A micrograph of the SAC/Au/Pd/Ni/Cu couple reacted at 270 °C for 1 h is presented in Fig. 1(b). Two different layers could be fund at the interface. A gray, irregular, and thick region close to the SAC solder can be observed, which composition is Sn–33.4Cu–22.4Ni (at.%) in the (Cu, Ni)$_6Sn_5$ phase [17]. This indicates that 22.4 at.% of the Ni atoms dissolve in IMC phase. Furthermore, the dark and thin region near the Cu side is the Cu_3Sn phase with the composition of Cu–22.7 at.% Sn [15].

Fig. 3(a) shows a larger area of an optical micrograph of the un-etched SAC/Au/Pd/Ni/Cu couple reacted at 270 °C for 1 h, in which the massive spalling of the (Cu, Ni)$_6Sn_5$ phase can be observed. The zoom-in SEI image of Fig. 3(a) is shown in Fig. 3(b). Fig. 3(c) and (d) shows the local magnitude image of Fig. 3(b). The composition ratio of the (Cu, Ni)$_6Sn_5$ phases, as shown in Fig. 3(c), closed to the SAC solder side is $(Cu_{0.77}Ni_{0.23})_6Sn_5$. The grain morphology shows a loose stack among the grains and irregular polyhedron-type shape. The composition ratio of the (Cu, Ni)$_6Sn_5$ phases close to the Cu side, as shown in Fig. 3(d), is $(Cu_{0.96}Ni_{0.04})_6Sn_5$. The morphology of the (Cu, Ni)$_6Sn_5$ phase is smooth, which is similar to a cobble-type of the Cu_6Sn_5 phase, owing to the lesser amount of Ni dissolved in the (Cu, Ni)$_6Sn_5$ phase. Different amounts of Ni contents dissolved into (Cu, Ni)$_6Sn_5$ phase resulted in different grain morphologies. Many small and spherical-type grains were found adhered to the surface of the (Cu, Ni)$_6Sn_5$ phases, as shown in Fig. 3(c) and (d). However, the composition could not be analyzed using EDS or EPMA, because the grain size was too small. It is presumed that the Ag_3Sn phase precipitated and deposited onto the (Cu, Ni)$_6Sn_5$ phase surface during the SAC solder solidification process.

When the reaction temperatures were reduced to 255 and 240 °C or when the reaction time was extended to 4 h, the (Cu, Ni)$_6Sn_5$ and Cu_3Sn phases were still formed at the interface, and a part of the (Cu, Ni)$_6Sn_5$ phase progressively peeled off from the interface. The peeling-off phenomenon induced by the Cu microelement in the SAC solder is considered to be caused by the Cu in the SAC solder diffusing into the interface and replacing Ni to react with Sn. Subsequently, the (Cu, Ni)$_6Sn_5$ phase is formed. This reaction mechanism is similar to that found by Ho et al. [12], in that both Ni_3Sn_4 and Cu_6Sn_5 phases were formed at the Sn–Ag–*x*Cu/Ni interface, when the value of *x* was between 0.4 and 0.5 wt%. However, the Ni atoms in this case finitely dissolved and reacted with the Sn and Cu atoms from the solder. Furthermore, the (Ni, Cu)$_3Sn_4$ phase was only found under shorter reaction time and lower reaction temperature conditions.

3.3. Sn–0.7Cu/Au/Pd/Ni/Cu reaction couple

Fig. 1(c) shows a BEI micrograph of the SC/Au/Pd/Ni/Cu couple reacted at 270 °C for 1 h. The charcoal, continuous and plane phases can be found at the Cu side. The composition revealed by EPMA analysis is Cu–23.9 at.% Sn in the Cu_3Sn phase [15]. The composition of the light gray, irregular, thick phase at the SC side is Sn–44.7Cu–7.9Ni (at.%), which is the (Cu, Ni)$_6Sn_5$ phase [7]. These results are similar to that found in He et al's study [20]. Furthermore, the Cu_3Sn and (Cu, Ni)$_6Sn_5$ phases were still formed in the SC/Au/Pd/Ni/Cu couple, reacted at 250 and 240 °C.

The (Cu, Ni)$_6Sn_5$ and Cu_3Sn phases were formed in the Sn/Au/Pd/Ni/Cu, SAC/Au/Pd/Ni/Cu and SC/Au/Pd/Ni/Cu couples. However, the (Cu, Ni)$_6Sn_5$ phase formed in the SC/Au/Pd/Ni/Cu couple peeled off severely from the substrate, toward the solder, when compared with the Sn/Au/Pd/Ni/Cu and SAC/Au/Pd/Ni/Cu

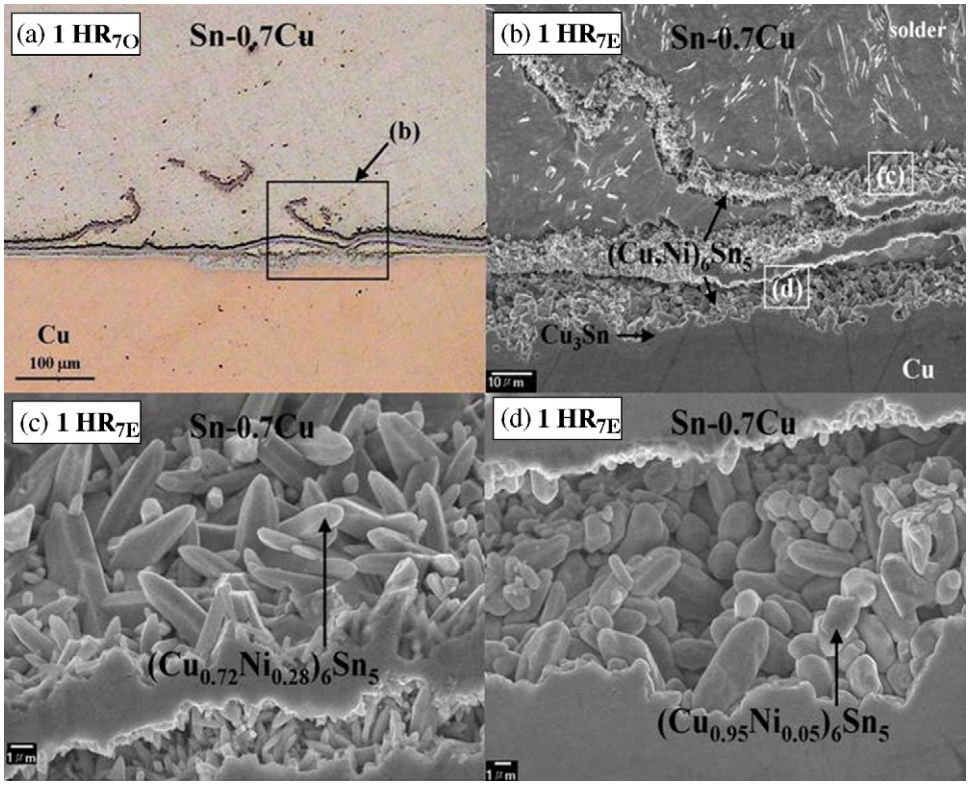

Fig. 4. (a) Un-etched optical micrograph and (b) deep-etched BEI micrograph of the SC/Au/Pd/Ni/Cu reaction couple reacted at 270 °C for 1 h; (c), (d) is magnified locally from (b).

couples. This peeling-off phenomenon was induced by negligible Cu content in the solder. The (Cu, Ni)$_6$Sn$_5$ phase was stably formed in the solder/Ni/Cu couple when the Cu content in the solder was greater than 0.5 wt% [12]. The small grain size of the (Cu, Ni)$_6$Sn$_5$ phases ripened together to form the (Cu, Ni)$_6$Sn$_5$ phases with larger grain size. These larger (Cu, Ni)$_6$Sn$_5$ phases peeled off from the interface and spread over the solder. There was a significant grain ripening process when the reaction time was extended to 4 h, and this mechanism was also observed in the Sn/Au/Pd/Ni/Cu and SAC/Au/Pd/Ni/Cu system.

Fig. 4(a) shows an un-etched OM image of the SC/Au/Pd/Ni/Cu couple at 270 °C for 1 h, and Fig. 4(b) shows the SEI microstructure of the image presented in Fig. 4(a) after etching. This region is the peeling-off IMC. Fig. 4(c) and (d) shows the local magnified images presented in Fig. 4(b). The composition of the (Cu, Ni)$_6$Sn$_5$ phase above the interface close to the SC solder was (Cu$_{0.72}$Ni$_{0.28}$)$_6$Sn$_5$, as shown in Fig. 4(c). The grain morphology was a polyhedron-type column structure with needle-like tails. When compared with the (Cu, Ni)$_6$Sn$_5$ phase in the SAC/Au/Pd/Ni/Cu system, the (Cu, Ni)$_6$Sn$_5$ phase close to the SC solder side was densely stacked along with the grains. The composition of the (Cu, Ni)$_6$Sn$_5$ phase near the Cu substrate side was (Cu$_{0.95}$Ni$_{0.05}$)$_6$Sn$_5$, as shown in Fig. 4(d). The morphology was smooth and plane, similar to the cobble-like grain of the Cu$_6$Sn$_5$ phase, which may be owing to the lesser Ni contents dissolved in the (Cu, Ni)$_6$Sn$_5$ phase. These results are similar to that of the SAC/Au/Pd/Ni/Cu couples. The different Ni concentration in the (Cu, Ni)$_6$Sn$_5$ phase resulted in a different morphology for the (Cu, Ni)$_6$Sn$_5$ phase.

3.4. Sn–58Bi/Au/Pd/Ni/Cu reaction couple

Fig. 5(a) shows a BEI micrograph of the SB/Au/Pd/Ni/Cu couple reacted at 270 °C for 1 h. The dark and light color layers in the SB solder are (Sn) and (Bi) phases, respectively. A light-colored plane IMC layer was found at the interface with a composition of Sn–38.3Ni–2.2Pd–1.9Cu (at.%) in the Ni$_3$Sn$_4$ phase [16]. The layer close to the Cu side, showing dark and regular morphology, is the remnant Ni layer. When the reaction temperatures were reduced to 255 and 240 °C, only the Ni$_3$Sn$_4$ phase was formed at the solder/substrate interface. This result is consistent with that observed in Wang's study [21]. Furthermore, only the Ni$_3$Sn$_4$ phase could be found for the liquid-solid interfacial reaction between the Sn–Bi solder and Ni substrate.

Owing to the large Bi concentration in the SB solder system, the Sn diffusion rate toward the substrate solder could be suppressed.

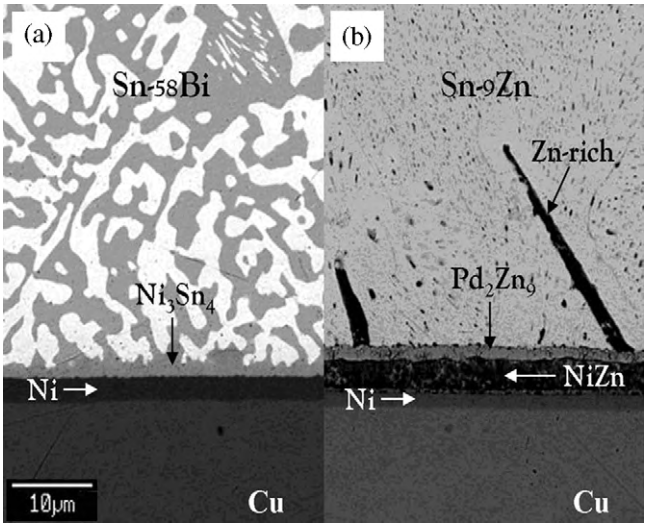

Fig. 5. BEI micrograph of the (a) SB, and (b) SZ/Au/Pd/Ni/Cu reaction couples reacted at 270 °C for 1 h.

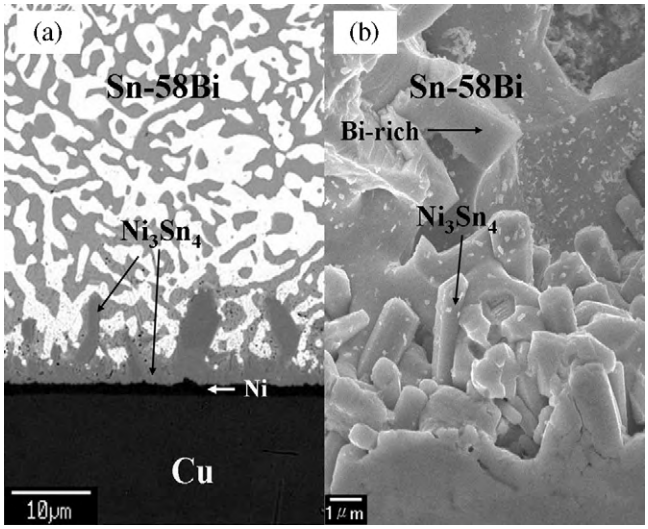

Fig. 6. (a) Un-etched and (b) deep-etched BEI microstructure of the SB/Au/Pd/Ni/Cu reaction couple reacted at 270 °C for 4 h.

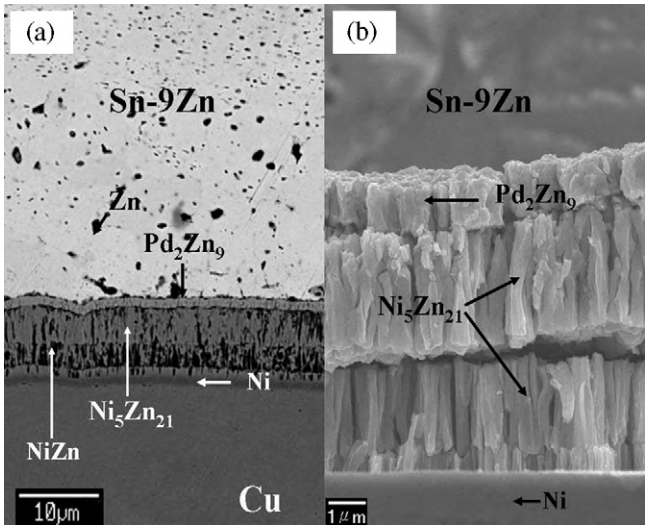

Fig. 7. (a) Un-etched and (b) deep-etched BEI microstructure of the SZ/Au/Pd/Ni/Cu reaction couple reacted at 270 °C for 4 h.

Thus, Sn atoms could diffuse slowly toward the Ni layer and progressively consume them to form the Ni_3Sn_4 phase at the interface. This Ni layer acts as a diffusion barrier to prevent the Sn atoms from diffusing toward the Cu side to form the Cu–Sn IMCs. Therefore, the major IMC formed at the interface is the Ni_3Sn_4 phase. As shown in Fig. 6(a), the thickness of the Ni_3Sn_4 phase increased significantly when the reaction time was increased to 4 h. However, the Ni layer remained at the interface. Fig. 6(b) presents a deep-etched SEI image of the SB/Au/Pd/Ni/Cu couple reacted at 270 °C for 4 h. Larger pieces of the Bi-rich phase were exposed in the solder and the microstructure of the Ni_3Sn_4 phase was a needle-like grain with compact stacking.

3.5. Sn-9Zn/Au/Pd/Ni/Cu reaction couple

Fig. 5(b) shows the BEI image of SZ/Au/Pd/Ni/Cu couple reacted at 270 °C for 1 h. A dark black, needle-like region in the SZ solder is the (Zn) phase, and the charcoal gray and plane layer near the Cu side is the remnant Ni layer. Two different colored layers between the SZ solder and Ni layer could be obviously observed. The continuous, smooth layer close to the SZ solder has a light gray color and is thin. According to EPMA quantitative analysis, its composition is Zn–14.5Pd–2.7Cu–1.1Ni (at.%), and is in the Pd_2Zn_9 phase [15]. However, this was different from that observed in other solder/Au/Pd/Ni/Cu reaction couples. The planar layer between the Pd_2Zn_9 phase and Ni layer had a dark black color and smooth morphology, and its composition is Zn–46.1 at.% Ni in the NiZn phase [16,22].

When the reaction time was extended to 4 h, the thickness of the Pd_2Zn_9 phase, when compared with that presented in Fig. 5(b), did not increase obviously, as shown in Fig. 7(a). This indicates that the Pd layer completely reacted with the Zn layer with no extra Pd left to form a thicker Pd_2Zn_9 phase. Three planar layers with a light gray color and black column-like regions among the layers between the Pd_2Zn_9 phase and Ni layer can also be found in Fig. 7(a). The composition of the light gray layers is Zn–17.1Ni–2.1Cu (at.%) in the Ni_5Zn_{21} phase [16], and the black color region is the NiZn phase. This result is different from that in which the couple reacted for 1 h. Furthermore, it was observed that extending the reaction could change the IMC formation.

The reaction mechanism is that the Zn atoms have higher activity, and can easily aggregate to the interface and react with the substrate. At the initial reaction stage, the thin Au layer rapidly dissolves into the solder [24] and the Pd layer remains intact. The Zn atoms come in direct contact with the Pd layer, and then react with Pd to form the Pd_2Zn_9 phase. However, the Zn atoms continuously diffuse through the Pd_2Zn_9 phase toward the Ni layer. At this stage, not many Zn atoms reach the Ni side. Thus, the NiZn phase, which has the low stoichiometry number of Zn/Ni, is first formed at the interface. As the diffusion rate of the Zn atom is faster than that of the Ni atom [19], extending the reaction time can allow more Zn atoms to diffuse toward the Ni side. However, the Ni supply is limited, and the NiZn phase is progressively converted to the Ni_5Zn_{21} phase with the increasing reaction time. This result is similar to that observed by Chou, indicating that Ni_5Zn_{21} is formed at the interface of the Sn–9Zn/Ni and Sn–9Zn–1Cu/Ni systems [23].

Fig. 7(b) shows a deep-etched SEI image of SZ/Au/Pd/Ni/Cu couple reacted at 270 °C for 4 h. The upper Pd_2Zn_9 phase and the Ni_5Zn_{21} phase can be observed. Furthermore, the grain morphology of the Pd_2Zn_9 phase is irregular stacking to one layer and the Ni_5Zn_{21} has a column-type stack to three layers.

3.6. Kinetics of the interfacial reaction

The total thickness of the IMC layers increases when the reaction time and temperature are increased. A linear relationship for each reaction couple exists between the thickness of all IMCs and the square root of the reaction time. Their growth rates can be described by the parabolic law, and the IMC growth is diffusion-controlled.

The linear relationship between the thickness of the IMCs and the square root of the reaction time is described by $x = kt^{1/2}$, where k is the growth-rate constant. From the Arrhenius equation, $k = k_0\exp(-Q/RT)$, the growth-rate constant (k) and the activation energy (Q) can be determined and are listed in Table 2. As shown in Fig. 8, the Sn–58Bi/Au/Pd/Ni/Cu system has the lowest growth-

Table 2
Growth-rate constants and activation energy and for each couple.

System	Growth-rate constant $k \times 10^{15}$ m^2 s^{-1}			Q (kJ/mol)
	240 °C	255 °C	270 °C	
Sn/Au/Pd/Ni/Cu	58.54	82.41	113.87	51.4
SAC/Au/Pd/Ni/Cu	66.30	89.62	118.32	44.7
SC/Au/Pd/Ni/Cu	75.11	106.02	140.84	48.6
SB/Au/Pd/Ni/Cu	0.67	0.76	0.84	17.4
SZ/Au/Pd/Ni/Cu	3.73	4.30	4.95	21.8

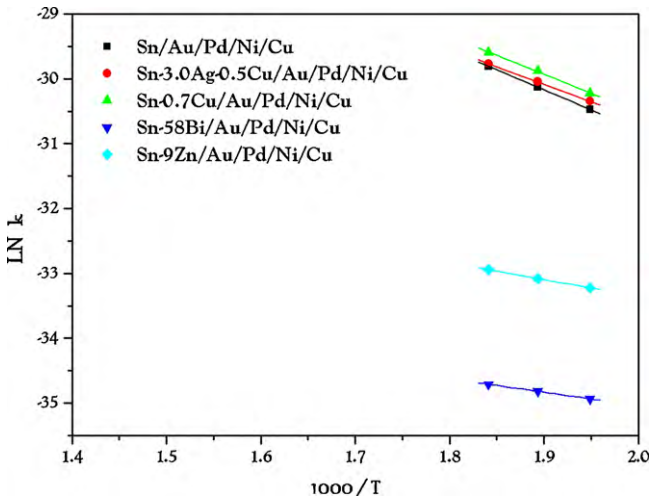

Fig. 8. Arrhenius plot for the formation of IMC in solder/Au/Pd/Ni/Cu couples.

rate constant, when compared with other systems owing to the fact that only the Ni_3Sn_4 phase is found for the liquid–solid interfacial reaction of the SB/Au/Pd/Ni/Cu system. Furthermore, the activation energy value of the Sn–58Bi/Au/Pd/Ni/Cu system is 17.43 kJ/mol.

4. Conclusions

This study investigated the interfacial reactions between Sn, SAC, SC, SB and SZ Pb-free solders with Au/Pd/Ni/Cu multilayer substrates at 240–270 °C for various reaction times. The experimental results presented that the $(Ni, Cu)_3Sn_4$ phase was formed in the Sn/Au/Pd/Ni/Cu system when the reaction time was less than 4 h. Both the $(Cu, Ni)_6Sn_5$ and Cu_3Sn phases were formed in the Sn/Au/Pd/Ni/Cu, SAC/Au/Pd/Ni/Cu, and SC/Au/Pd/Ni/Cu systems. In the SB/Au/Pd/Ni/Cu system, only the Ni_3Sn_4 phase was formed at the solder/substrate interface. The Pd_2Zn_9 and NiZn phases were formed in the SZ/Au/Pd/Ni/Cu system. As the reaction time was increased, more Zn atoms diffused toward the substrate and reacted with the Ni atoms. Thus, the Pd_2Zn_9 and NiZn phase and as well as the Ni_5Zn_{21} phase were formed at the interface. The reaction mechanism for all the reaction systems was diffusion-controlled, and the SB/Au/Pd/Ni/Cu system had the lowest growth-rate constant and activation energy, when compared with other systems.

Acknowledgments

The authors acknowledge the financial support of the National Science Council of Taiwan, Republic of China (Grant nos. NSC 97-2221-E-011-080 and 98-2221-E-011-042) and are grateful to Mr. C. Y. Kao for carrying out the EPMA analysis and Mr. Laiw for carrying out the FE-SEM analysis.

References

[1] S.W. Chen, Y.W. Yen, J. Electron. Mater. 28 (1999).
[2] J.W. Yoon, S.B. Jung, J. Alloys Compd. 396 (2005).
[3] M.D. Settle, C.C. Patterson, Science 207 (1980).
[4] C.H. Wang, S.W. Chen, Acta Mater. 54 (2006).
[5] J.W. Yoon, S.B. Jung, J. Alloys Compd. 359 (2003).
[6] J.W. Yoon, S.W. Kim, S.B. Jung, J. Alloys Compd. 385 (2004).
[7] J.W. Yoon, S.W. Kim, S.B. Jung, J. Alloys Compd. 392 (2005).
[8] C.Y. Lee, J.W. Yoon, Y.J. Kim, S.B. Jung, Microelectron. Eng. 82 (2005).
[9] J.W. Yoon, S.W. Kim, S.B. Jung, J. Alloys Compd. 415 (2006).
[10] W.H. Tao, C. Chen, C.E. Ho, W.T. Chen, C.R. Kao, Chem. Mater. 13 (2001).
[11] W.T. Chen, C.E. Ho, C.R. Kao, J. Mater. Res. 17 (2002).
[12] C.E. Ho, R.Y. Tsai, Y.L. Liu, C.R. Kao, J. Electron. Mater. 31 (2002).
[13] C.E. Ho, Y.W. Lin, S.C. Yang, C.R. Kao, J. Electron. Mater. 35 (2006).
[14] S.K. Kang, D.Y. Shih, K. Fogel, P. Lauro, M.J. Yim, G. Advocate, M. Griffin, C. Goldsmith, D.W. Henderson, T. Gosselin, D. King, J. Konrad, A. Sarkhel, K.J. Puttlitz, IEEE 25 (2002).
[15] H. Baker (Ed.), ASM Handbook-Alloy Phase Diagram, ASM International, Materials Park, Ohio, 1990.
[16] H. Baker (Ed.), ASM Handbook-Alloy Phase Diagram, ASM International, Materials Park, Ohio, 2006.
[17] C.H. Lin, S.W. Chen, C.H. Wang, J. Electron. Mater. 31 (2002).
[18] F. Bartels, J.W. Morris, G. Dalke, W. Gust, J. Electron. Mater. 23 (1994).
[19] B.F. Dyson, T.R. Anthony, D. Turnbull, J. Appl. Phys. 38 (1967).
[20] D.P. He, D.Q. Yu, W. Lai, C.M. Lawrence, Chin. J. Nonferrous Met. 16 (2006).
[21] J. Wang, H.F. Liu, L.B. Liu, Z.P. Jin, J. Electron. Mater 35 (2006).
[22] C.Y. Chou, PhD. Thesis, National Tsing-Hua University (2006).
[23] C.Y. Chou, S.W. Chen, Y.S. Chang, J. Mater. Res. 21 (2006).
[24] C.E. Ho, Y.M. Chen, C.R. Kao, J. Electron. Mater. 28 (1999).